Inter*net* Electronic Journal of Molecular Design

November 2004, Volume 3, Number 11, Pages 684–703

Editor: Ovidiu Ivanciuc

Inhibition of Xanthine–Oxidase by 2,4–Dihydroxy–Benzophenone and 2,3,4–Trihydroxy–Benzophenone

Gabriela T. Castro,[1] Sonia E. Blanco,[1] and Ferdinando H. Ferretti [1]

[1] Area de Química–Física, Facultad de Química, Bioquímica y Farmacia, Universidad Nacional de San Luis, Chacabuco y Pedernera, 5700 San Luis, Argentina

Received: February 16, 2004; Revised: July 27, 2004; Accepted: September 3, 2004; Published: November 30, 2004

Citation of the article:
G. T. Castro, S. E. Blanco, and F. H. Ferretti, Inhibition of Xanthine–Oxidase by 2,4–Dihydroxy–Benzophenone and 2,3,4–Trihydroxy–Benzophenone, *Internet Electron. J. Mol. Des.* **2004**, *3*, 684–703, http://www.biochempress.com.

Inter*net* Electronic Journal of Molecular Design

BioChem Press
http://www.biochempress.com

Inhibition of Xanthine–Oxidase by 2,4–Dihydroxy–Benzophenone and 2,3,4–Trihydroxy–Benzophenone

Gabriela T. Castro,[1] Sonia E. Blanco,[1] and Ferdinando H. Ferretti [1,*]

[1] Area de Química–Física, Facultad de Química, Bioquímica y Farmacia, Universidad Nacional de San Luis, Chacabuco y Pedernera, 5700 San Luis, Argentina

Received: February 16, 2004; Revised: July 27, 2004; Accepted: September 3, 2004; Published: November 30, 2004

Internet Electron. J. Mol. Des. **2004**, *3* (11), 684–703

Abstract

Motivation. Xanthine oxidase is a very important enzyme that catalyzes the oxidation of xanthine to uric acid, which plays a crucial role in gout. The search for new compounds that are capable of inhibiting the activity of XO therefore constitutes a field of investigation that attracts great interest. As a continuation of studies performed on benzophenones, in this work we determine the inhibition of XO by 2,4–dihydroxybenzophenone and 2,3,4–trihydroxybenzophenone. We propose a model for the representation of the active site of XO, which was used to describe the possible enzyme–substrate and enzyme–inhibitor interactions.

Method. The IC_{50} of the compounds was determined using a UV–visible spectroscopic kinetic method. Basis sets at B3LYP/6–31+G(d) and HF/3–21G were used for performing the calculations that permitted to describe the interactions involving the enzyme, the substrate and the inhibitors.

Results. The IC_{50} data obtained indicate that 2,4–dihydroxybenzophenone and 2,3,4–trihydroxybenzophenone exert a moderate inhibiting activity on XO, which is comparable to that exhibited by other polyphenolic BPs, but is lower to that of potent inhibitors of XO like allopurinol or quercetin. On the other hand, a model for the active site of XO was proposed, which includes a pentaheteroatomic ring and two extracyclic heteroatoms (S and O). The structures of the enzyme–substrate and enzyme–inhibitor–complex were calculated using this model.

Conclusions. The inhibition of XO by 2,4–dihydroxybenzophenone and 2,3,4–trihydroxybenzophenone is produced by a Michaelis–Menten mechanism of the competitive reversible type. It was also established that the inhibiting activity of the compounds is determined by the stability of the enzyme–inhibitor complex and is independent of their acidity constants.

Keywords. Xanthine oxidase; inhibiting activity of benzophenones; inhibitor–enzyme interactions; mechanism; *ab initio* and DFT calculations.

Abbreviations and notations

BPs, benzophenones	K_a, acid ionization constant
XO, xanthine oxidase	K_F, formation constant of the enzyme–drug complex
X, xanthine	PEC, potential energy curve
TRIS, tris(hydroxymethyl)aminomethane	IHB, intramolecular hydrogen bond
DMSO, dimethylsulphoxide	DM, dipole moment
DFT, density functional method	*A*, bond angle
TE, total energy	*r*, bond length
D, dihedral angle	ASXO, active site model of XO
U, uric acid	

* Correspondence author; phone: 54–2652–423789; fax: 54–2652–430224; E–mail: fferret@unsl.edu.ar.

1 INTRODUCTION

Benzophenones (BPs) are matter of continuous biological and industrial investigations due to their insecticide [1], platelet–aggregation inhibiting [2], UV radiation absorbing [3] and enzyme inhibiting (xanthine oxidase) [4] properties, among others. On the other hand, xanthine oxidase (XO) is a fundamental oxomolybdoenzyme [5] in the human purines metabolism. The inhibition of XO is very important because this enzyme catalyzes the oxidation of xanthine (X) to uric acid [6], which plays a crucial role in gout [7].

The demonstration that XO is involved in free radical production [8] led to an increasing interest in the study of other enzyme properties and related topics. Thus, advances have been made on adsorptive properties (size and molecular area) in bovine milk [9], the increase of antioxidant activity and XO inhibition of catechin by enzymatic polymerization [10], the microfabrication of bioreactor chips for immobilized enzyme assays [11], the X–ray absorption spectroscopy of a structural analogue of the oxidized active sites in the sulfite oxidase enzyme family and related molybdenum (V) complexes [12], as well as the redox interplay of oxo–thio–tungsten centers with sulfur–donor co–ligands [13].

On the other hand, although information on the quantitative inhibition of XO for BPs is scarce [4], the kinetic study of the inhibition degree of this enzyme by polyphenolic BPs, and the probable anti–oxidizing properties of these compounds with potential pharmaceutical applications is of major interest. In this work kinetic experiments of enzymatic inhibition were carried out with the main purpose of accurately determining the inhibition degree of XO by 2,4–dihydroxy–benzophenone (**1**) and 2,3,4–trihydroxy–benzophenone (**2**). In addition, and taking into account that for many pharmacological agents the main mechanism of action involves drug–enzyme interactions, as in the case of XO inhibition by allopurinol [14,15], to explain the relative inhibitory capability of **1** and **2**, we also analyze theoretically the possible interactions of these compounds and of X, with the catalytic center of XO by means of *ab initio* a DFT methods.

2 MATERIALS AND METHODS

2.1 Reagents

Compounds **1** and **2** from Sigma Chemical Co were purified by repeated crystallization from ethanol–water mixtures. Purity control was performed determining their melting points [16] (mp(**1**) = 144ºC, mp(**2**) = 140–141ºC) as well as their thin–layer chromatographic and UV–visible spectroscopic properties [17]. X and XO (EC 1.1.3.22, grade IV from bovine milk) were obtained from Sigma Chemical Co. The enzymatic preparation of XO contains 4.37 U/mL. Dimethylsulphoxide (DMSO), used to dissolve the BPs, was purchased from Merck and employed without further purification.

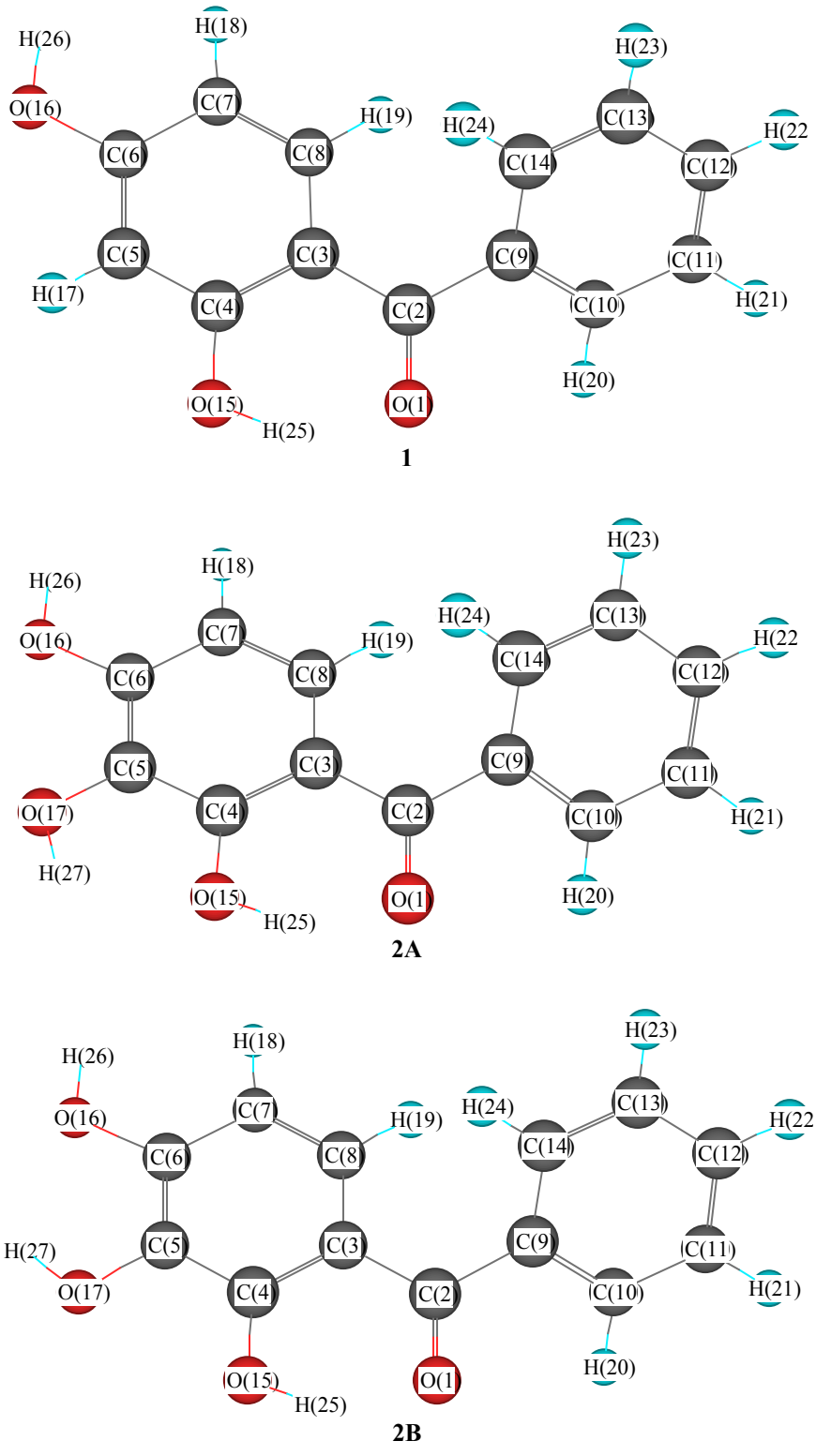

Figure 1. Structure and practical numbering system adopted in the calculations of the hydroxy–benzophenones studied. (**1**) 2,4–dihydroxy–benzophenone; (**2A**) First conformer of 2,3,4–dihydroxy–benzophenone; (**2B**) Second conformer of 2,3,4–dihydroxy–benzophenone.

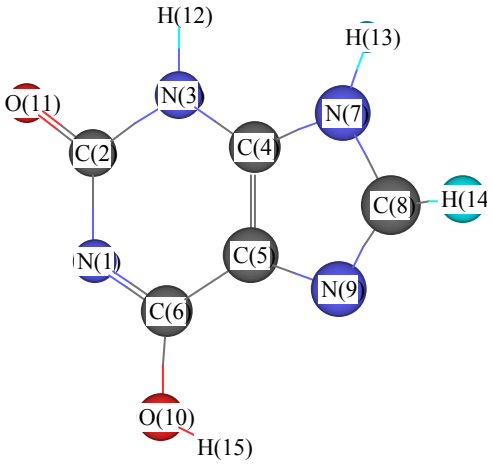

Figure 2. Lactim structure of xanthine and practical numbering system used in the calculations.

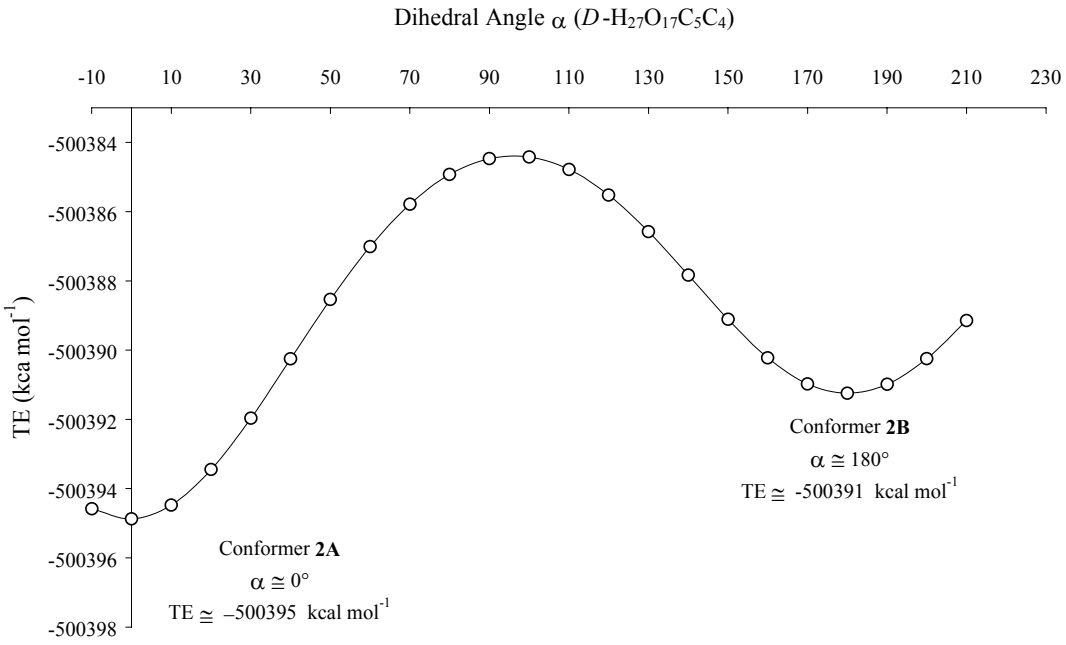

Figure 3. Potential energy curve for the hydroxyl group bound to C_5 (ring A) of 2,3,4–trihydroxy–benzophenone, computed at HF/6–31+G(d) in vacuum, at 298 K.

2.2 Experimental Procedures

Preliminary experiments of XO inhibition were carried out in order to select the best working conditions. The concentration of X was 2.71×10^{-5} mol L^{-1} in TRIS buffer (5×10^{-3} mol L^{-1} pH 8.1). BPs **1** and **2** were added to the reaction mixture dissolved in DMSO. The final concentration of DMSO in the reaction medium was 0.34% (v/v). The inhibition of XO was determined by monitoring the formation of urate at 290 nm, on a Shimadzu UV 160A double beam spectrophotometer with 1 cm thermostatically controlled cells, at 303.0 K. In the procedure followed for quantitative determinations, 2.9 mL reaction mixtures were prepared containing X (2.71×10^{-5} mol L^{-1}) and BP (**1** or **2**) in variable concentrations (between 1.69×10^{-5} and 1.07×10^{-4} mol L^{-1}). The reaction was initiated by adding 3μL of XO solution and the absorbances were read

every 5 seconds for 10 min. Control experiments (without BP) were carried out simultaneously. The percent inhibition degree was calculated with Eq. (8).

2.3 Calculations

The structure and practical numbering system adopted in the calculations of the hydroxy–benzophenones studied are shown in Figure 1. Figure 2 shows the lactim structure of X and corresponding practical numbering system. The structure of **1** has been recently analyzed in vacuum and water [18], with the B3LYP/6–31G(d) method. In this work, the stereochemical characteristics of **1** and **2** and the molecular properties of the monoanions of both BPs were determined at HF/6–31+G(d) and B3LYP/6–31+G(d). For the determination of the potential energy curve (PEC) of **2** in vacuum at HF/6–31+G(d) (Figure 3), the total energy (TE) of molecular structures were calculated as a function of the dihedral angle α using 10º increments in the −10° to 210º interval. It was proposed that dihedral angle α (Figure 1, *D*–$H_{27}O_{17}C_5C_4$) is formed by the plane containing the hydroxyl group bound to C_5 and the plane containing the rest of the substituted aromatic ring A of the molecule. The two planes intersect along the single bond O_{17}–C_5. The potential energy curve minima obtained by the scan of **2** (Figure 3) were optimized with the Gaussian 98 [19] program packages, using the HF/6–31G+(d) and B3LYP/6–31+G(d) methods and the default convergence criteria. Tomasi's [20] method was used to analyze the solvent effects on all the species studied as well as the conformational equilibrium constant that involves conformers **2A** and **2B**.

On the other hand, considering that molybdenum (atomic number 42) is outside the range of most standard basis sets used by the programs included in the Gaussian 98 package, the study of the drug–enzyme interactions was carried out at HF/3–21G. Moreover, the specific calculations to obtain the molecular properties of the inhibitor–enzyme complex in water were performed with the Tomasi's method using the uahf atomic radii [21].

3 RESULTS AND DISCUSSION

The mechanism by which molybdenum enzymes such as XO carry out substrate hydroxylation has been the subject of continued interest. Thus, the crystal structure of XO from bovine milk has been reported recently [22]. The active sites of these enzymes have the basic structure $LMo^{VI}OS(OH)$, where L represent a pyranopterin cofactor common to all mononuclear molybdenum and tungsten enzymes; this ligand binds to the metal via a side chain with and RC(SH)=C(SH)R' structure. The coordination geometry is square pyramidal, with Mo=O, Mo–OH, and pyranopterin in the equatorial plane and Mo=S in the apical position.

The available evidence favor a mechanism in which and active site base (proposed to be a conserved glutamate residue, [22]) abstracts the proton from the Mo–OH group, initiating

nucleophilic attack on substrate with concomitant hydride transfer from C–8 of substrate to the Mo=S. This yield an $LMo^{IV}O(SH)(OR)$ species, where OR represents product coordinated to the metal via the newly introduced hydroxyl group. Voityut *et al*. [23], by density functional calculations has considered a mechanism for the transformation of a substrate (choosing formaldehyde) at the Mo center (Figure 4, adapted from ref [23]).

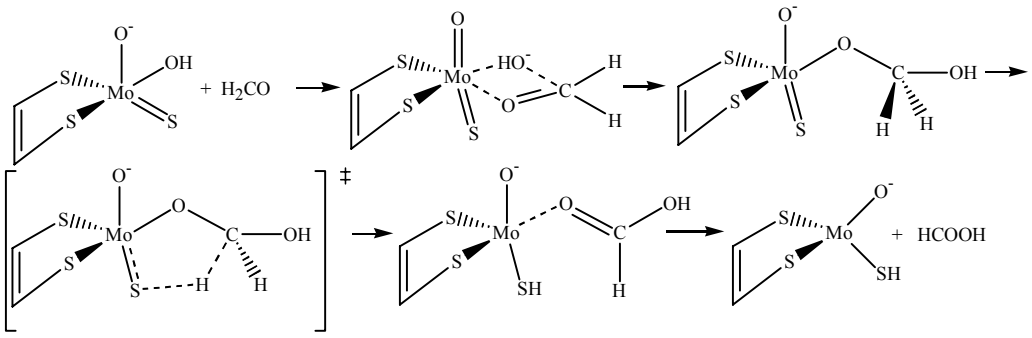

Figure 4. Reaction mechanism of xanthine oxidase (adapted from Ref. [23]).

Competitive inhibition

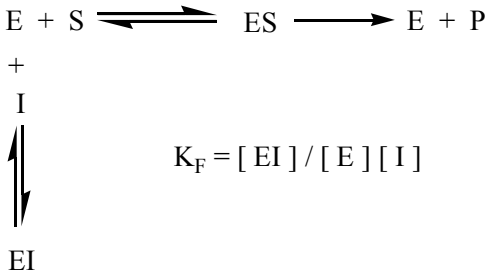

Figure 5. Competitive inhibition mechanism of xanthine oxidase.

These molybdenum enzymes catalyze the transfer of an oxygen atom between water and a substrate, which may rang from an aromatic heterocycle (*e.g*., xanthine) to a simple aldehyde. This oxygen transfer is coupled to a two–electron redox reaction. The catalytic reaction can be thought of as proceeding in two half–cycles. Within the first (reductive) half cycle, the oxidation of a substrate occurs at the Mo site, accompanied by a reduction of the metal center from Mo(VI) to Mo(IV). In the course of the second (oxidative) half cycle, the Mo(IV) state is regenerate due to two one–electron transfer processes from the molybdenum center to the other redox–active cofactors (*e.g*., to the FAD cofactor in XO) [24,25]. On the other hand, Stockert *et al*. [26] have realized kinetic studies using a homologous series of substrates and concluded that XO most likely operates via two–electron chemistry, with formation of the initially appearing $LMo^{IV}O(SH)(OR)$ intermediate in a single two–electron process involving nucleophilic attack on substrate followed by hydride transfer to the molybdenum center.

For its great importance XO has been under investigation for decades and numerous inhibitors of this enzyme were informed, such as allopurinol [15], pteridines [27], phytic acid [28], flavonoids

[29–31] and medicinal plants used to treat the gout [32]. In particular, for flavonoids, the structure–function relationships have been discussed [30] and different types of inhibition mechanisms have also been reported. For example, Van Hoorn *et al*. [31] reported competitive inhibition (Figure 5) by quercetin and mixed–type inhibition by morin and galangin. Cotelle *et al*. [33], reported noncompetitive inhibition for 3',4',5'–trihydroxyflavone, and competitive inhibition for luteolin and two 7–hydroxyflavones. The results of these authors suggest that these flavonoids inhibit XO activity not only by competitive mode, but also by interaction with the enzyme at a site other than the active center. Further detailed work is needed to clarify inhibition mechanism by flavonoids and related compounds. Recently, Lin *et al*. [34], to obtain more stereochemical data of the interactions of flavones on XO, have performed a study based on molecular modeling. As occurs with apigenin, the most potent inhibition ability it is associated with the most favorable interaction in the reactive site. Thus, the bicyclic benzopyranone ring of apigenin stacked with phenyl of Phe 914, and the phenolic group stretched to the space surrounding with several hydrophobic residues.

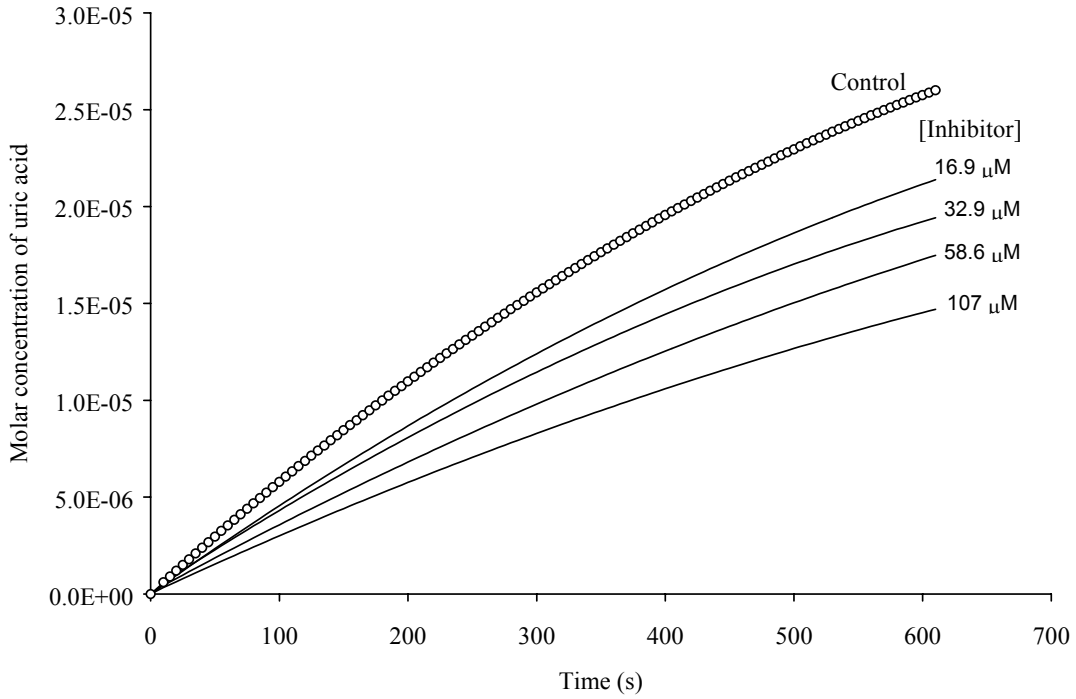

Figure 6. Variations of the molar concentration of uric acid as a function of the time of reaction, for a control experiment and four experiments with 2,3,4–trihydroxy–benzophenone added to the reaction medium.

3.1 Initial Rates

Considering only the species that absorb radiation at 290 nm, the oxidation reaction of X to uric acid (U) by XO, can be expressed as,

$$X \rightarrow U \tag{1}$$

The global reaction rate (V, mol L^{-1} s^{-1}) of the above reaction is

$$V = \frac{d[U]}{dt} = k_{obs}\,[X] \tag{2}$$

where t is the reaction time (s), [U] and [X] are the molar concentrations of U and X at any time, and k_{obs} is the pseudo first order rate constant (s^{-1}). Using Beer's law, the following expression was obtained,

$$[U] = \frac{A_t - A_0}{\varepsilon_U - \varepsilon_X} \tag{3}$$

In the above equation, A_t is the total solution absorbance; A_o is initial solution absorbance (t=0), and ε_U and ε_X are the molar absorptivities (L mol^{-1} cm^{-1}) of U and X, respectively. As an example, Figure 6 shows the variations of [U] as a function of the reaction time, for a control experiment and four experiments with inhibitor **2** added to the reaction medium. As expected, when the concentration of **2** in the reaction medium increased, the progress of the enzyme–catalyzed reaction and the corresponding initial rates decreased.

According to Hall *et al*. [35], [U] may be formulated by means of powers of time, such as:

$$[U] = B_0 + B_1\,t + B_2\,t^2 + B_3\,t^3 + ... \tag{4}$$

In the above equation, B_o, B_1, B_2, etc. are numeric coefficients that can be easily determined by non–linear regression [36]. By deriving Eq. (4) with respect to time,

$$V = \frac{d[U]}{dt} = B_1 + 2B_2\,t + 3B_3\,t^2 + ... \tag{5}$$

When t = 0, it is clear that:

$$B_1 = \left(\frac{d[U]}{dt}\right)_{t=0} = V_0 \tag{6}$$

Eq. (6) indicates that the B_1 coefficient is equal to V_o (mol L^{-1} s^{-1}), *i.e*., the initial rate of the enzymatic reaction. The V_o of all the kinetic experiments performed was calculated by this procedure.

3.2 Percent Inhibition Degree and IC_{50}

In order to explain XO inhibition by BPs and taking into account the results of additional experiments carried out in our laboratory, it is reasonable to suggest that this inhibition takes place by a Michaelis–Menten mechanism of the competitive reversible type, as occurs with the inhibition of XO by flavones [33]. It must be noted that several flavones with varied biological activities present hydroxyl groups in positions similar to the BPs here studied [37,38]. The rate equation for the mentioned mechanism is:

$$V_0 = \frac{V_{max}\,[X]_0}{K_M\,(1 + K_F\,[BP]_0) + [X]_0} \tag{7}$$

where V_o and V_{max} are the initial and maximum rates (mol L^{-1} s^{-1}) of the enzymatic reaction, respectively; $[X]_o$ and $[BP]_o$ are the initial molar concentrations (mol L^{-1}) of X (substrate) and BP (inhibitor), respectively, K_M is the Michaelis–Menten constant and K_F is the formation constant of the enzyme–inhibitor complex.

On the other hand, to analyze quantitatively XO activity inhibition by BPs, the percent inhibition degree (PID), was defined as

$$PID = \frac{V_{0C} - V_0}{V_{0C}} \times 100 \tag{8}$$

where V_{oC} is the initial rate (mol L^{-1} s^{-1}) of the control enzymatic reaction ([BP]=0) and V_o is the initial rate of the enzymatic reaction in presence of the inhibitor. From Eqs. (7) and (8), the following expression was obtained:

$$\frac{PID}{100 - PID} = \frac{K_M\,[BP]_0\,K_F}{K_M + [X]_0} \tag{9}$$

By definition, magnitude IC_{50} is the concentration of inhibitor required to produce 50% inhibition in an enzyme–catalyzed reaction. Consequently, from Eq. (9) it is inferred that:

$$IC_{50}\,(BP) = \frac{K_M + [X]_0}{K_M\,K_F} \tag{10}$$

If in the experiments of enzymatic inhibition by BPs the same concentrations [BP] and $[X]_o$ are used, it becomes clear that:

$$IC_{50}\,(BP) = \frac{Q}{K_F} \tag{11}$$

where Q is a constant. The previous equation indicates that the BP that forms the most stable enzyme–drug complex, *i.e.*, a complex with a high K_F value, will have the greatest XO inhibiting activity.

Table 1 summarizes the results of the experiments of XO inhibition by **1** and **2**. This Table includes the molar concentrations of substrate and inhibitor used in the experiments, and the corresponding values of V_o, PID and IC_{50}. It must be noted that according to Eq. (11), the IC_{50} values obtained suggest that the constant K_F (**2**) should be greater than K_F (**1**). Furthermore, it should also be observed that the IC_{50} values of **1** and **2** are high compared with those exhibited by potent inhibitors of XO like allopurinol (IC_{50} = 10.66 μM) or 3,5,7,3',4'$(OH)_5$–flavone (quercetin, IC_{50} = 7.23 μM) [4].

Table 1. Results of the experiments of XO inhibition by 2,4$(OH)_2$–benzophenone and 2,3,4$(OH)_3$–benzophenone. $[X]_o$ = initial molar concentration of xanthine; $[BP]_o$ = initial molar concentration of inhibitor (**1** and **2**); V_o = initial global rate (mol L^{-1} s^{-1}), Eq. (6); PID = percent inhibition degree, Eq. (8); IC_{50} = Concentration of inhibitor required to produce 50% inhibition in the enzymatic reaction (μmol L^{-1})

Run	$[X]_o$	$[BP]_o$	2,4$(OH)_2$–Benzophenone			2,3,4$(OH)_3$–Benzophenone		
			V_o	PID	IC_{50}	V_o	PID	IC_{50}
1	$2.71\ 10^{-5}$	0	$6.087\ 10^{-8}$	0		$6.087\ 10^{-8}$	0	
2	$2.71\ 10^{-5}$	$1.686\ 10^{-5}$	$5.469\ 10^{-5}$	10.16	184 μM	$4.739\ 10^{-8}$	22.14	112 μM
3	$2.71\ 10^{-5}$	$3.287\ 10^{-5}$	$4.832\ 10^{-5}$	20.61		$4.171\ 10^{-8}$	31.48	
4	$2.71\ 10^{-5}$	$5.859\ 10^{-5}$	$4.256\ 10^{-5}$	30.08		$3.651\ 10^{-8}$	40.02	
5	$2.71\ 10^{-5}$	$10.73\ 10^{-5}$	$3.627\ 10^{-5}$	40.41		$3.081\ 10^{-8}$	49.39	

Table 2. Calculated structural magnitudes at B3LYP/6–31+G(d) for 2,4$(OH)_2$–Benzophenone (**1**) and the conformers (**2A**, **2B**) of 2,3,4$(OH)_3$–Benzophenone (**2**) in vacuum, at 298 K. ΔG_f^o = Standard energy of formation, cal mol^{-1}; K_{C2}= Conformational equilibrium constant, Eq. (12); DM = dipolar moment (Debye); a_0 = molecular radii, Å; *D*–$O_1C_2C_3C_4$ = dihedral angle $O_1C_2C_3C_4$ (º); *D*–$H_{26}O_{16}C_6C_5$ = dihedral angle $H_{26}O_{16}C_6C_5$ (º); *q* = total atomic charge (Mulliken), a.u.; *d*O_1–H_{25}, *d*O_{15}–H_{27}, *d*O_{16}–H_{27} = distance of the intramolecular hydrogen bond between the indicated atoms, Å (Figure 1); *A*-$O_1H_{25}O_{15}$, *A*-$O_{15}H_{27}O_{17}$, *A*-$O_{16}H_{27}O_{17}$ = H–bond angles (º)).

Magnitude	Vacuum		
	1	**2A**	**2B**
ΔG_f^o	–8515	–9231	–9326
K_{C2}	–	1.17	
DM	5.24	4.76	6.20
a_0	4.75	5.04	5.02
D–$O_1C_2C_3C_4$	10.7	10.2	11.4
D–$H_{26}O_{16}C_6C_5$	179.2	179.2	178.6
qO_1	–0.503	–0.489	–0.484
qO_{16}	–0.667	–0.660	–0.769
qH_{26}	0.481	0.490	0.508
dO_1–H_{25}	1.682	1.677	1.691
A–$O_1H_{25}O_{15}$	147.1	146.1	146.7
dO_{15}–H_{27}	–	2.125	–
A–$O_{15}H_{27}O_{17}$	–	113.5	–
dO_{16}–H_{27}	–	–	2.163
A–$O_{16}H_{27}O_{17}$	–	–	112.3

3.3 Conformational Properties of Benzophenones

It is well–known that the number of conformers of a compound depends on the number of rotatable bonds it possesses [39]. Thus, BP **2** has one more pair of conformers than BP **1**. The existence of these conformers of **2** was detected by rotation of the plane that involves the $O_{17}H_{27}$ group bound to C_5 and the plane containing the rest of the substituted aromatic ring A (Figure 1, dihedral angle α = *D*–$H_{27}O_{17}C_5C_4$) around the single bond C_5–$O_{17}H_{27}$. Figure 3 shows the calculated potential energy curve (PEC) in vacuum at HF/6–31+G(d). In the interval –10° to 210º, it can be observed that the PEC exhibits two different energy minima, characterized by dihedral angles α = 0º and α = 180º. The energy of the involved rotation barrier (RBE) is 7.31 kcal mol^{-1}, approximately. As in a previous work [40], it was proposed that the following conformational equilibrium exists between **2A** and **2B**,

$$\mathbf{2\,A} \Leftrightarrow \mathbf{2\,B} \qquad (12)$$

which is characterized by the conformational equilibrium constant K_{C2}. Tables 2 and 3 summarize the optimized values of molecular properties of 2,4–dihydroxy–benzophenone and the conformers (**2A**, **2B**) of 2,3,4–trihydroxy–benzophenone (Figure 1) obtained at B3LYP/6–31+G(d) at 298 K, in vacuum and water, respectively.

Table 3. Calculated structural magnitudes using the Tomasi's method at B3LYP/6–31+G(d) for 2,4$(OH)_2$–benzophenone (**1**) and the conformers (**2A**, **2B**) of 2,3,4$(OH)_3$–benzophenone (**2**) in water, at 298 K. G^o_{sol} = total free energy in solution, kcal mol^{-1}; K_{C2} = conformational equilibrium constant, Eq. (12); DM = dipolar moment (Debye); v = molecular volume, $Å^3$; *D*–$O_1C_2C_3C_4$ = dihedral angle $O_1C_2C_3C_4$ (º); *D*–$H_{26}O_{16}C_6C_5$ = dihedral angle $H_{26}O_{16}C_6C_5$ (º); *q* = total atomic charge (Mulliken), a.u.; *d*O_1–H_{25}, *d*O_{15}–H_{27}, *d*O_{16}–H_{27} = distance of the intramolecular hydrogen bond between the indicated atoms, Å (Figure 1); *A*–$O_1H_{25}O_{15}$, *A*–$O_{15}H_{27}O_{17}$, *A*–$O_{16}H_{27}O_{17}$ = H–bond angles (º)).

Magnitude	Water		
	1	**2A**	**2B**
G^o_{sol}	–456276	–503480	–503479
K_{C2}	–	0.185	
DM	7.88	7.13	9.41
v	227.02	233.94	234.43
D–$O_1C_2C_3C_4$	10.7	10.2	11.4
D–$H_{26}O_{16}C_6C_5$	179.2	179.2	178.6
qO_1	–0.594	–0.586	–0.580
qO_{16}	–0.738	–0.757	–0.822
qH_{26}	0.553	0.565	0.576
dO_1–H_{25}	1.682	1.677	1.691
A–$O_1H_{25}O_{15}$	147.1	146.1	146.7
dO_{15}–H_{27}	–	2.125	–
A–$O_{15}H_{27}O_{17}$	–	113.5	–
dO_{16}–H_{27}	–	–	2.163
A–$O_{16}H_{27}O_{17}$	–	–	112.3

Our data indicate that the substituted aromatic ring A of **1**, **2A** and **2B** have a practically planar structure, while the total molecules possess non–planar structures. This is due to the fact that the plane containing the unsubstituted aromatic ring B forms an inclination angle (θ) of 47.8–49.0° with the plane that comprises the rest of the molecule. These two planes intersect along the single bond C_2–C_9 (Figure 1). The data of Tables 2 and 3 reveal that in solution, the relative thermodynamic stability of the **2A** and **2B** conformers is opposite to that observed in vacuum. Furthermore, practically all geometrical parameters of the compounds calculated in vacuum and in water are identical. This implies that the solvent does not affect the molecular geometry of **1**, **2A** and **2B**. On the contrary, the Mulliken's atomic charges (*q*) and corresponding dipole moments (DM) show important variations between the values calculated in vacuum and those calculated in water. This means that the polarity of the solvent increases the *q* (in absolute value) and DM of the species. On the other hand, it must be noted that the solvent decreases K_{C2}. Consequently, it can be concluded that the conformational reaction described by Eq. (12) is not favored by the solvent. This fact is reflected on the theoretical values of K_C. The K_{C2} value obtained in water (K_{C2} = 0.185) is 6.3 times smaller than the calculated value in vacuum (K_{C2} = 1.17). Moreover, the value K_{C2} = 0.185

indicates that in aqueous medium at 298 K there exists 84.4% of **2A** and 15.4% of **2B** in equilibrium. This means that in water conformer **2A** is the predominant form of **2**. Consequently, we shall consider only this compound to represent BP **2** in all the discussions that follow.

3.4 Inhibitory and Acid–Base Properties of Flavones and Benzophenones

All flavones with high inhibiting activity on XO exhibit an α,β–unsaturated carbonyl group and OH groups at positions 7 and 5 [37,41]. The 7 and 5 positions of flavones are equivalent, respectively, to the *para* and *ortho* positions of the investigated BPs in this work.

Table 4. Calculated structural properties using the Tomasi's method at HF/3–21G for the anions 4(O^-),2(OH)–benzophenonate (**1**$^-$), 4(O^-)2,3($OH)_2$–benzophenonate (**2A**$^-$), (O_{10}^-)–xanthinate (**X**$^-$) in water, at 298 K. G^o_{sol} = total free energy in solution, kcal mol^{-1}; K_a = acid dissociation constant, Eqs. (13) and (14); ΔG_{solva} = free energy of solvation, kcal mol^{-1}; v = molecular volume, $Å^3$; *D*–$O_1C_2C_3C_4$ = dihedral angle $O_1C_2C_3C_4$ (º); *D*–$O_{16}C_6C_5C_4$ = dihedral angle $O_{16}C_6C_5C_4$ (º); *q* = total atomic charge (Mulliken), a.u.; *d*O_1–H_{25}, *d*O_{15}–H_{27} = distance of the intramolecular hydrogen bond between the indicated atoms, Å; *A*–$O_1H_{25}O_{15}$, *A*–$O_{15}H_{27}O_{17}$ = H–bond angles (º)).

Magnitude	**X**$^-$ (Figure 2)	**1**$^-$ (Figure 1)	**2A**$^-$ (Figure 1)
G^o_{sol}	–348659	–450683	–497395
ΔG_{solva}	–79.66	–54.76	–57.74
K_a	$3.80\ 10^{-11}$	$2.35\ 10^{-16}$	$1.51\ 10^{-16}$
v	161.01	270.84	278.60
D–$O_1C_2C_3C_4$	–	9.7	9.2
D–$O_{16}C_6C_5C_4$	–	179.6	179.6
D–$C_6N_1C_2N_3$	0.0	–	–
D–$C_4N_7C_8N_9$	0.0	–	–
qO_1	–	–0.747	–0.744
qO_{16}	–	–0.807	–0.791
qO_{10}	–0.758	–	–
dO_1–H_{25}	–	1.677	1.680
A–$O_1H_{25}O_{15}$	–	145.9	145.1
dO_{15}–H_{27}	–	–	2.093
A–$O_{15}H_{27}O_{17}$	–	–	114.7

Cotelle *et al*. [33] determined that several 7–hydroxy–flavones are potent competitive inhibitors of XO and proposed that the OH group at position 7 of flavones may take the place of the HO groups bonded to C_2 or C_6 of X (Figure 2) in the active site of the enzyme. Costantino *et al*. [42,43] synthesized and tested a new series of 7–hydroxyflavones as XO inhibitors and concluded that: (*a*) in solution, there exists an equilibrium between the neuter and dissociated forms of the compounds; (*b*) the flavones act as donors of electrons in the interaction with the enzyme by means of the anionic forms that were originated from proton dissociation of the group HO–C_7. Other authors [41] also proposed that a planar structure is important for inhibition of XO.

Taking into account the notable structural similarity that exists between the substituted aromatic rings A of biologically active flavones and those of **1** and **2A**, we shall assume that the knowledge on bioactivity–structure relationships developed for the mentioned flavones can be applied to these compounds. From the structures of **1** and **2A** (Figure 1), it can be observed that the H_{26} atom of the

hydroxyl (O_{16}–H_{26}) group bound to C_6 (*para*–position of ring A) is more acidic than the H_{25} atom of the hydroxyl (O_{15}–H_{25}) group bound to C_4 (*ortho*–position of ring A), due to the strong intramolecular hydrogen bond (IHB) that characterizes all *o*–hydroxy–benzophenones [44]. The referred IHB involve to the *o*–hydroxyl and carbonyl groups of these compounds. On the other hand, the OH groups attached to two adjacent carbon atoms C_4 and C_5 of **2A** also form an IHB, which specifically involves the H_{27} atom of the hydroxyl (O_{17}–H_{27}) group and the oxygen atom of the hydroxyl (O_{15}–H_{25}) group. These facts help to explain that the H_{26} atom of hydroxyl (O_{16}–H_{26}) of the *p*–position of **1** and **2A** is the most acidic hydrogen of all the hydroxyl groups. Consequently, we shall assume that the *p*–monoanionic forms of BP **1** (**1**$^-$) and BP **2A** (**2A**$^-$) are their active forms, this is to say, that the *p*–monoanions **1**$^-$ and **2A**$^-$ are those that have interactions with the active sites of XO.

Table 4 summarizes the calculated molecular properties for **1**$^-$ and **2A**$^-$ at HF/3–21G in water, at 298 K. It also includes the calculated properties for the lactim anion of X, 10(O^-)–xanthinate (Figure 2), which we shall represent as **X**$^-$. The first ionization constants (K_a) of **1** and **2A** were calculated by means of the conventional equations,

$$\mathbf{1} + H_2O \Leftrightarrow \mathbf{1}^- + H_3O^+ \tag{13}$$

$$\mathbf{2A} + H_2O \Leftrightarrow \mathbf{2A}^- + H_3O^+ \tag{14}$$

From Table 4 it can be observed that the substituted aromatic rings A of **1**$^-$ and **2A**$^-$ practically possess a planar structure, as occurs with the corresponding neuter molecules. Thus, the values of the dihedral angles *D*–$O_1C_2C_3C_4$ and *D*–$O_{16}C_6C_5C_4$ are close to 0° and 180°, respectively. However, the total molecules of these anions have non–planar structures. The two principal planes containing the A and B aromatic rings of **1**$^-$ (or **2A**$^-$) form an inclination angle θ of 44.6° (or 44.2°) with each other. These θ values reveal that the **1**$^-$ and **2A**$^-$ possess a higher coplanarity between their rings A and B with respect to **1** and **2A** (θ ≅ 48º). Moreover, it can also be noted that the geometric parameters and atomic charges which characterize **1**$^-$ and **2A**$^-$ are very similar. Likewise, the K_a values obtained for both compounds allow to conclude that the acidity of the H_{26} atom of the *p*–OH groups is approximately equivalent. On the other hand, it can also be observed that **X**$^-$ has a totally planar structure. All its dihedral angles are equal to zero. Moreover, the K_a constant of X indicates that the acidity of the H_{15} atom of $O_{10}H_{15}$ group bonded to C_6 is higher than those of the H_{26} atom of **1** and **2A**.

3.5 Interactions in the Active Site Model of XO

It is well–known that the molybdenum cofactor (Mo·molybdopterin) of XO has one oxo ligand and one sulfide ligand. The crystalline structure of the molybdenum cofactor reported by several authors [45–47] is shown in Figure 7, while the structural model of the catalytic center of XO proposed by Romão *et al*. [48] and Degtyarenko *et al*. [49] is shown in Figure 8.

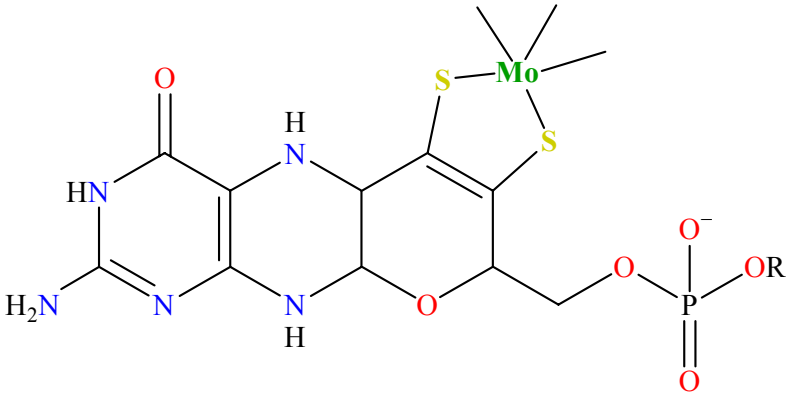

Figure 7. Molybdenum cofactor (Mo·molybdopterin). R = H (eukaryotic enzymes), AMP, CMP, GMP (prokaryotic enzymes).

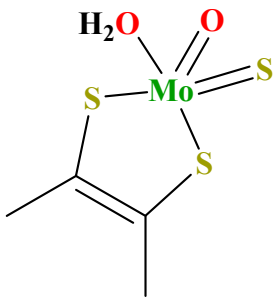

Figure 8. Molybdenum active site of XO ([MoSO](S$_{molybdopterin}$)$_2$ H_2O).

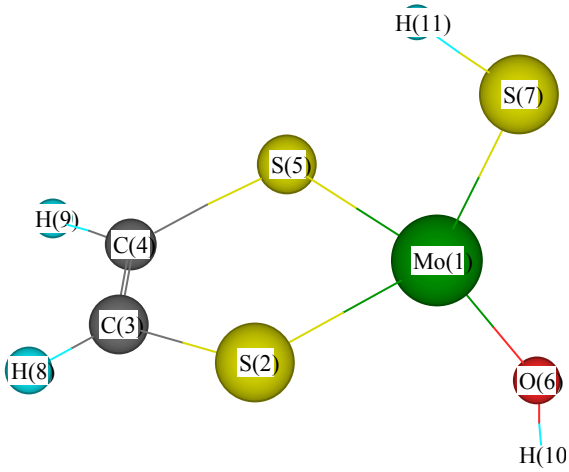

Figure 9. Model of the active site of XO proposed to analyze the inhibitor–enzyme interactions at HF/3–21G in water at 298 K.

The theoretical methods of the Gaussian 98 program packages do not permit to analyze the polycoordinated molybdenum atom with the geometry square pyramidal and double bonds that characterize the real active site of XO (Figure 8). For this reason, it was necessary to propose a simpler model for the active site of XO (ASXO), as the one shown in Figure 9. This model comprises a pentaheteroatomic ring, which includes two sulfur atoms of the thiophene type, and two extracyclic heteroatoms (a thiol–type sulfur atom and a hydroxyl oxygen atom). Obviously, the

model proposed for ASXO has been simplified with regard to the real model (Figure 8). However, it is useful for describing the conformational differences between the free and complexed **1**$^-$ and **2A**$^-$ anions at HF/3–21G as well as for explaining the different inhibiting capability on XO of these compounds.

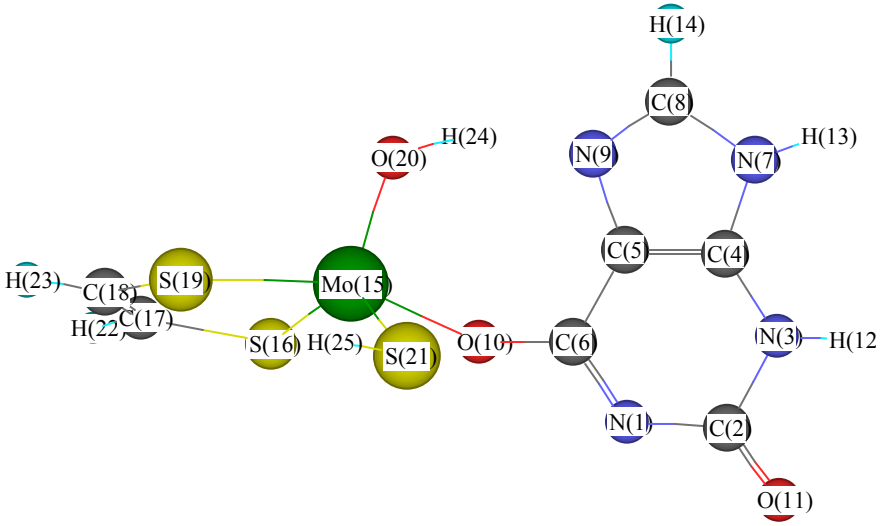

Figure 10. Calculated structure at HF/3–21G in water at 298 K, for the complex formed between the 10(O$^-$)–xanthinate anion and the active site model of XO.

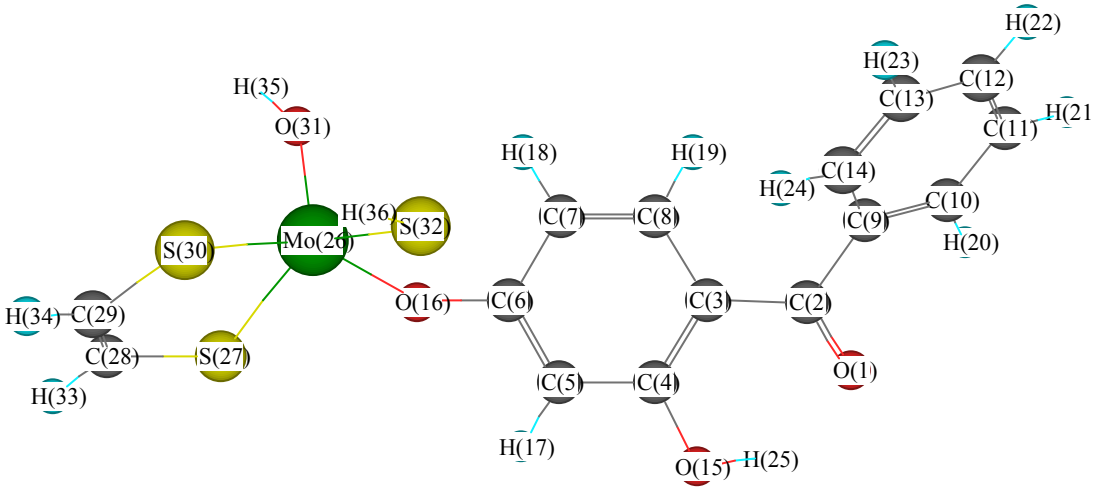

Figure 11. Calculated structure at HF/3–21G in water at 298 K, for the complex formed between the 4(O$^-$)–2(OH)–benzophenonate monoanion and the active site model of XO.

It was previously suggested that XO inhibition by BPs takes place by a Michaelis–Menten mechanism of the competitive reversible type (Eq. (7)). Consequently, and considering the above discussion, it is clear that **1**$^-$ and **2A**$^-$ compete with **X**$^-$ when interacting with the ASXO. Furthermore, from Eq. (11) it was inferred that the XO inhibiting activity of an inhibitor is large when it forms a complex of high thermodynamic stability with the ASXO. Table 5 gives the molecular magnitudes that characterize the free ASXO and the enzyme–drug complexes formed between the ASXO and the **X**$^-$, **1**$^-$ and **2A**$^-$ anions. As an example, Figures 10 and 11 show the

structures of the ASXO–**X**$^-$ and ASXO–**2A**$^-$, respectively. These structures were calculated at HF/3–21G, in water at 298 K.

Table 5. Calculated structural magnitudes using the Tomasi's method at HF/3–21G for the free active site model of XO (ASXO) and for the complexes formed between the ASXO and the 10(O^-)–xanthinate (**X**$^-$), 4(O^-)–2(OH)–benzophenonate (**1**$^-$) and 4(O^-)–2,3($OH)_2$–benzophenonate (**2A**$^-$) anions in water, at 298 K. G^o_{sol} = total free energy in solution, kcal mol^{-1}; K_F = equilibrium constant of formation of the complexes ASXO–substrate or ASXO–inhibitor; v = molecular volume, $Å^3$; *D*–$O_1C_2C_3C_4$ = dihedral angle $O_1C_2C_3C_4$ (º); *D*–$O_{16}C_6C_5C_4$ = dihedral angle $O_{16}C_6C_5C_4$ (º); *D*–$C_6N_1C_2N_3$ = dihedral angle $C_6N_1C_2N_3$ (º); *D*–$C_4N_7C_8N_9$ = dihedral angle $C_4N_7C_8N_9$ (º); *D*–$MoS_2C_3C_4$ = dihedral angle $MoS_2C_3C_4$ (º); *q* = total atomic charge (Mulliken), a.u.; *r*Mo–O_6, *r*Mo–S_7, *r*Mo–O_{10}, *r*Mo–O_{16} = bond length between the indicated atoms, Å; *A*–O_6MoS_7 = bond angle between the indicated atoms (º)).

Magnitude	ASXO (Figure 9)	ASXO–**X**$^-$	ASXO–**1**$^-$	ASXO–**2A**$^-$
G^o_{sol}	–3323024	–3671747	–3773773	–3820485
K_F	–	$4.68\ 10^{46}$	$1.53\ 10^{48}$	$1.69\ 10^{48}$
v	215.21	357.45	472.70	477.86
D–$O_1C_2C_3C_4$	–	–	14.4	13.3
D–$O_{16}C_6C_5C_4$	–	–	177.8	178.0
D–$C_6N_1C_2N_3$	–	0.4	–	–
D–$C_4N_7C_8N_9$	–	0.0	–	–
D–$MoS_2C_3C_4$	6.1	11.3	11.5	12.2
qO_1	–	–	–0740	–0724
qO_{16}	–	–	–0.864	–0.850
qO_{10}	–	–0.820	–	–
*q*Mo	1.108	1.071	1.093	1.080
qO_6	–0.786	–0.798	–0.798	–0.785
qS_7	–0.450	–0.505	–0.510	–0.531
*r*Mo–O_6	1.814	1.807	1.823	1.824
*r*Mo–S_7	2.385	2.462	2.471	2.480
A–O_6MoS_7	124.1	110.4	110.6	110.3
*r*Mo–O_{10}	–	2.056	–	–
*r*Mo–O_{16}	–	–	2.004	2.032
A–$MoO_{10}C_6$	–	142.8	–	–
A–$MoO_{16}C_6$	–	–	139.5	139.2

From a joint analysis of the data from Tables 4 and 5 the following can be concluded:

(*a*) The molecular volume of the enzyme–substrate or enzyme–inhibitor complexes is approximately 5% lower than the sum of the molecular volumes of the species that form these complexes.

(*b*) In the ASXO–**X**$^-$ complex, the **X**$^-$ moiety maintains the totally free structure of the free **X**$^-$ anion. However, in the ASXO–**1**$^-$ and ASXO–**2A**$^-$ complexes, the structure of the BPs suffers some changes. For example, the coplanarity of the carbonyl group with ring A is lower (by approximately 4–5°) than that exhibited in the **1**$^-$ and **2A**$^-$ free anions.

(*c*) The coplanarity of the pentaheteroatomic ring of the complexed ASXO also decreases by 5–6° with respect to the free ASXO. The dihedral angle *D*–$MoS_2C_3C_4$ (Figure 9) increases as follows:

$$\text{Free ASXO} < \text{ASXO–}\mathbf{X}^- < \text{ASXO–}\mathbf{1}^- < \text{ASXO–}\mathbf{2A}^- \quad (15)$$

The above ordering matches that exhibited by the K_F constants, *i.e.*, the formation equilibrium constants of the respective complexes. The K_F values increase as follows:

$$K_F\ (ASXO–\mathbf{X}^-) < K_F\ (ASXO–\mathbf{1}^-) < K_F\ (ASXO–\mathbf{2A}^-) \quad (16)$$

(*d*) From Table 4 it can be observed that the acid ionization constants of the compounds vary as follows:

$$K_a\ (\mathbf{X}) >> K_a\ (\mathbf{1}) \text{ and } K_a\ (\mathbf{2A})\ ; \qquad K_a\ (\mathbf{1}) > K_a\ (\mathbf{2A}) \quad (17)$$

(*e*) The atomic charges of the main atoms of ASXO, $\mathbf{X}^-$, $\mathbf{1}^-$ and $\mathbf{2A}^-$ in their free forms suffer random changes when the referred species form the enzyme–substrate or enzyme–inhibitor complexes. An obvious exception is seen in the extracyclic sulfur atom of ASXO, the charge of which (qS_7, Figure 9) increases in its absolute value as follows:

$$qS_7\ (ASXO) < qS_7\ (ASXO–\mathbf{X}^-) < qS_7\ (ASXO–\mathbf{1}^-) < qS_7\ (ASXO–\mathbf{2A}^-) \quad (18)$$

(*f*) The length of the bonding between the central atom and the extracyclic sulfur atom varies in a similar fashion to that described in the above equation. From Table 5, it can be observed that:

$$r\text{Mo–}S_7\ (ASXO) < r\text{Mo–}S_7\ (ASXO–\mathbf{X}^-) < r\text{Mo–}S_7\ (ASXO–\mathbf{1}^-) < r\text{Mo–}S_7\ (ASXO–\mathbf{2A}^-) \quad (1)$$

Considering Eqs. (11) and (16), it can be theoretically concluded that: (1) The fact that the K_F (ASXO–$\mathbf{1}^-$) and K_F (ASXO–$\mathbf{2A}^-$) constants are greater that K_F (ASXO–$\mathbf{X}^-$) reveals that the investigated BPs might hinder the oxidation of X by XO; (2) Similarly, since K_F ($\mathbf{2A}^-$) > K_F ($\mathbf{1}^-$), it is clear that the inhibiting capacity of $\mathbf{2A}^-$ is greater than that of $\mathbf{1}^-$. These conclusions totally match our experimental determinations (Table 1).

Considering Eqs. (18) and (19), it may be inferred that of the two extracyclic atoms of ASXO (O and S), the sulfur atom plays a more important role. In addition, from Eq. (15), it can be concluded that the compound with the greatest inhibiting capacity on XO is that which, in its interaction with the enzyme, produces a greatest distortion of the pentaheteroatomic ring of ASXO.

On the other hand, it might be expected that the values of the K_a constants of the analyzed substrate and inhibitors directly correlate with their physico–chemical behavior. However, as shown by Eqs. (16) and (17), there is no simple relation between the K_a constants and the corresponding K_F constants. It might be argued that the strong solvation of $\mathbf{X}^-$ (ΔG_{solva}= –79.66 kcal mol^{-1}, Table 4) gives this anion an elevated stability in solution, which is markedly higher than that of $\mathbf{1}^-$ and $\mathbf{2A}^-$ ($\Delta G_{solva} \cong$ –55 to –58 kcal mol^{-1}). Yet, the elevated stability of $\mathbf{X}^-$ can strongly hinder its interaction with ASXO. On the other hand, the lower stability of $\mathbf{1}^-$ and $\mathbf{2A}^-$ in solution could facilitate and intensify the interactions between ASXO and the $\mathbf{1}^-$ and $\mathbf{2A}^-$ anions.

4 CONCLUSIONS

As part of a program aimed at investigating new biological and physicochemical properties of BPs, in this paper we determined the inhibition of XO by 2,4–dihydroxybenzophenone (**1**) and 2,3,4–trihydroxybenzophenone (**2**). Using X as substrate, it was determined that **1** and **2** inhibit the activity of XO by 40% and 50%, respectively. These inhibition percentages implicate that IC_{50} (**1**) = 184 μM and IC_{50} (**2**) = 112 μM. The obtained data of IC_{50} indicate that **1** and **2** exert a moderate inhibitory activity on XO, comparable to that exhibited by other polyphenolic BPs but lower than that of potent inhibitors of XO like allopurinol or 3,5,7,3',4'$(OH)_5$–flavone (quercetin). Furthermore, modification of enzyme kinetics equations permitted to conclude that the inhibition of XO by **1** and **2** is produced by means of a Michaelis–Menten mechanism of the competitive reversible type. The calculations performed at B3LYP/6–31+G(d) using Tomasi's method allowed to prove that in water 2,3,4–trihydroxy–benzophenone has two rotamers that depend on the position of the 3(OH) group. In addition to the strong molecular hydrogen bond (IHB) that characterizes all *o*–hydroxy–benzophenones, these conformers exhibit another IHB of moderate intensity that involves the OH groups attached to two adjacent carbon atoms (*meta* and *para* position). On the other hand, a model to represent the active site of XO was proposed that comprises a pentaheteroatomic ring and two extracyclic heteroatoms (S and O). The results obtained at HF/3–21G permit to suggest that the inhibitory activity of **1** and **2** is mainly determined by the stability of the enzyme–inhibitor complex and is independent of the acidity constants of the compounds. It was also concluded that the compound with the greatest inhibitory capacity on is the one that, in its interactions with the enzyme, produces the greatest variations of the coplanarity of the pentaheteroatomic ring of the enzyme active site model.

Acknowledgment

This work was supported by grants from National University of San Luis (Argentine Republic).

5 REFERENCES

[1] S. Budavari, The Merck Index 12th. ed. Merck & Co., NJ, 1996, p. 1125.
[2] J. Elks and C. R. Ganellin, *Dictionary of Drugs*, London, Chapman & Hall, 1990, pp. 413, 569, 628, 1238.
[3] P. Collins and J. Ferguson, Photoallergic contact dermatitis to oxybenzone, *Br. J. Dermat.* **1994**, *131*, 124–129.
[4] S. Y. Seu, H. J. Tsai and H. C. Chiang, Benzophenones as xanthine oxidase inhibitors, *Anticancer Res.* **1999**, *19*, 1131–1136.
[5] P. E. Baugh, D. Collison, C. D. Garner and J. A. Joule, *Molybdenum metalloenzymes*, in Comprehensive Biological Catalysis, 1998, Vol III, pp. 377–400.
[6] S. A. Holmer, C. L. Houlton and T. D. Westmoreland, A new irreversibly inhibited form of xanthine oxidase from ethylisonitrile, *J. Inorg. Biochem.* **1997**, *66*, 63–65.
[7] G. B. Elion, S. Callahan, H. Nathan, S. Bieber, R. W. Rundles and G. H. Hitching, Potentiation by inhibition of

drug degradation : 6–substituted purines and xanthine oxidase, *Biochem. Pharmacol*. **1963**, *12*, 85–93.
[8] J. M. McCord and I. Fridovich, The reduction of cytochrome c by milk xanthine oxidase, *J. Biol. Chem*. **1968**, *243*, 5753–5760.
[9] D. Kristensen, T. Nylander, J. T. Rasmussen, M. Paulsson and K. S. Birdi, Adsorbed and spread films of bovine milk xanthine oxidase at the air–water interface, *Colloids Surf. A–Phys. Eng. Aspects*. **1998**, *143*, 221–231.
[10] M. Kurisawa, J. E. Chung, Y.J. Kim, H. Uyama and S. Kobayashi, Amplification of antioxidant activity and xanthine oxidase inhibition of catechin by enzymatic polymerization, *Biomacromolec*. **2003**, *4*, 469–471.
[11] S. Banu, G. M. Greenway, T. McCreedy and R Shaddick, Microfabricated bioreactor chips for immobilised enzyme assays, *Anal. Chim. Acta*, **2003**, *486*, 149–157.
[12] F. Jalilehvand, B. S. Lim, R. H. Holm, B. Hedman and K. O. Hodgson, X–ray absorption spectroscopy of a structural analogue of the oxidized active sites in the sulfite oxidase enzyme family and related molybdenum(V) complexes, *J. Inorg. Chem*. **2003**, *42*, 5531–5536
[13] S. Thomas, A. A. Eagle, S. A. Sproules, J. P. Hill, J. M. White, E. R. T. Tiekink, G. N. George and C. G. Young, Redox interplay of oxo–thio–tungsten centers with sulfur–donor co–ligands, *J. Inorg. Chem*. **2003**, *42*, 5909–5916.
[14] A. S. Klein, J. W. Joh, U. Rangan, D. Wang and G. B. Bulkley, Allopurinol: Discrimination of antioxidant from enzyme inhibitory activities, *Free Radic. Biol. Med*. **1996**, *21*, 713–717.
[15] M. K. Shukla and P. C. Mishra, Electronic spectra and structure of allopurinol: A xanthine oxidase inhibitor, *Spectrochim. Acta Part A*. **1996**, *52*, 1547–1557.
[16] J. G. Grasselli, M. S. William and M. Ritcher (Eds), *Atlas of Spectral Data and Physical Constants for Organic Compounds*, Vol III, CRS Press Inc. NY, 1975, pp–b2600–b2664.
[17] B. Fried and J. Sherma, *Thin–Layer Chromatography* (*Chromatographic Science*, V. 81), 4th Ed, Marcel Dekker, USA, 1999.
[18] A. Mantas, S. E. Blanco and F. H. Ferretti, The effects of substituents and solvents on the conformation of benzophenones, *Internet Electron. J. Mol. Des*. **2004**, *3*, 387-399, http://www.biochempress.com.
[19] Gaussian 98, Revision A.9, M. J. Frisch, G. W. Trucks, H. B. Schlegel, G. E. Scuseria, M. A. Robb, J. R. Cheeseman, V. G. Zakrzewski, J. A. Montgomery, Jr., R. E. Stratmann, J. C. Burant, S. Dapprich, J. M. Millam, A. D. Daniels, K. N. Kudin, M. C. Strain, O. Farkas, J. Tomasi, V. Barone, M. Cossi, R. Cammi, B. Mennucci, C. Pomelli, C. Adamo, S. Clifford, J. Ochterski, G. A. Petersson, P. Y. Ayala, Q. Cui, K. Morokuma, D. K. Malick, A. D. Rabuck, K. Raghavachari, J. B. Foresman, J. Cioslowski, J. V. Ortiz, A. G. Baboul, B. B. Stefanov, G. Liu, A. Liashenko, P. Piskorz, I. Komaromi, R. Gomperts, R. L. Martin, D. J. Fox, T. Keith, M. A. Al–Laham, C. Y. Peng, A. Nanayakkara, M. Challacombe, P. M. W. Gill, B. Johnson, W. Chen, M. W. Wong, J. L. Andres, C. Gonzalez, M. Head–Gordon, E. S. Replogle, and J. A. Pople, Gaussian, Inc., Pittsburgh PA, 1998.
[20] S. Miertus and J. Tomasi, Approximate evaluations of the electrostatic free energy and internal energy changes in solution processes, *Chem. Phys*. **1982**, *65*, 239–245.
[21] V. Barone, M. Cossi and J. Tomasi, A new definition of cavities for the computation of solvation free energies by the polarizable continuum model, *J. Chem. Phys*. **1997**, *107*, 3210–3221.
[22] C. Enroth, B. T. Eger, K. Okamoto, T. Nishino and E. F. Pai, Crystal structure of bovine milk xanthine deshydrogenase and xanthine oxidase: structure–based mechanism of conversion, *Proc. Natl. Acad. Sci. U.S.A*., **2000**, *97*, 10723–10728.
[23] A. A. Voityuk, K. Albert, M. J. Romão, R. Huber and N. Rosch, Substrate oxidation in the active site of xanthine oxidase and related enzymes. A model density functional study, *J. Inorg. Chem*. **1998**, *37*, 176–180.
[24] R. Hille, The reaction mechanism of oxomolybdenum enzymes, *Biochim. Biophys. Acta*. **1994**, *1184*, 143–169.
[25] R. Hille, The reaction mechanism of xanthine oxidase, *J. Inorg. Chem*. **2003**, *96*, 52.
[26] A. L. Stockert, S. S. Shinde, R. F. Anderson and R. Hille, The reaction mechanism of xanthine oxidase: Evidence for two–electron chemistry rather than sequential one–electron steps, *J. Am. Chem. Soc*. **2002**, *124*, 14554–14555.
[27] K. Oettl and G. Reibnegger, Pteridines as inhibitors of xanthine oxidase: structural requirements, *Biochim. Biophys. Acta*. **1999**, *1430*, 387–395.
[28] S. Muraoka and T. Miura, Inhibition of xanthine oxidase by phytic acid and its antioxidative action, *Life Sci*, **2004**, *74*, 1691–1700.
[29] A. Nagao, M. Seki and H. Kobayashi, Inhibition of xanthine oxidase by flavonoids, *Biosci. Biotechnol. Biochem*. **1999**, *63*, 1787–1790.
[30] A. M. Ponce, S. E. Blanco, A. S. Molina, R. García–Domenech and J. Gálvez–Alvarez, Study of the action of flavonoids on xanthine–oxidase by Molecular Topology, *J. Chem. Inform. Comput. Sci*. **2000**, *40*, 1039–1045.
[31] D. E. C. Van Hoorn, R. J. Nijveldt, P. A. M. Van Leeuwen, Z. Hofman, L. M'Rabet, D. B. A. De Bont and K. Van Nor, Accurate prediction of xanthine oxidase inhibition based on the structure of flavonoids, *Eur. J. Pharmacol*. **2002**, *451*, 111–118.
[32] L. D. Kong, Y. Cai, W. W. Huang, C. H. K. Cheng and R. X. Tan, Inhibition of xanthine oxidase by some Chinese medicinal plants used to treat gout, *Ethnopharmacol*. **2000**, *73*, 199–207.

[33] N. Cotelle, J. L. Bernier, J. P. Catteau, J. Pommery, J. C. Wallet and E. M. Gaydou, Antioxidant properties of hydroxyl–flavones, *Free Radic*. *Biol*. *Med*. **1996**, *20*, 35–43.
[34] C. M. Lin, C. S. Chen, C. T. Chen, Y. C. Liang and J. K. Lin, Molecular modeling of flavonoids that inhibits xanthine oxidase, *Biochem*. *Biophys*. *Res*. *Comm*. **2002**, *294*, 167–172.
[35] K. J. Hall, T. I. Quickenden and D. W. Watts, Rate constants from initial concentration data, *J. Chem*. *Educ*. **1976**, *53*, 493–494.
[36] A. Cornish–Bowden. *Analysis of Enzyme Kinetic Data*, Oxford Univ. Press, Oxford, 1995, pp. 27–30.
[37] J. B. Harborne, *The Flavonoids*. *Advances in Research since 1986*, Chapman & Hall/CRC, N.Y. 1999, pp. 259–336.
[38] C. A. Rice–Evans and L. Packer, *Flavonoids in Health and Disease*, Marcel Dekker Inc., N.Y. 1998, pp. 199–219 and 437–446.
[39] C. O. Wilson and O. Gisvold's, *Textbook of Organic Medicinal and Pharmaceutical Chemistry*, 10th ed, Edit. J. N. Delgado and W. A. Remers, Lippincott–Raven Publishers, N.Y., 1998, pp. 3–42.
[40] R. A. Rudyk, M. A. A. Molina, M. I. Gómez, S. E. Blanco and F. H. Ferretti, Structure and dipole moment of catechol in hydroxylic solvents, *Internet Electron*. *J. Mol*. *Des*. **2004**, *3*, 11–28, http://www.biochempress.com.
[41] P. Cos, L. Ying, M. Calomme, P. Hu Jia, K. Cimanga, B. Van Poel, L. Pieters, A. J. Vlietinck and B. D. Vanden, Structure–activity relationship and classification of flavonoids as inhibitors of xanthine oxidase and superoxide scavengers, *J*. *Nat*. *Prod*. **1998**, *61*, 71–76.
[42] L. Costantino, G. Rastelli and A. Albasini, A rational approach to the design of flavones as xanthine oxidase inhibitors, *Eur*. *J. Med*. *Chem*. **1996**, *31*, 693–699.
[43] G. Rastelli, L. Costantino and A. Albasini, A model of the interaction of substrates and inhibitors with xanthine oxidase, *J*. *Am*. *Chem*. *Soc*. **1997**, *119*, 3007–3016.
[44] A. C. Bhasikuttan, A. K. Singh, D. K. Palit, A. V. Sapre and J. P. Mittal, Laser flash photolysis studies on the monohydroxy derivatives of benzophenone, *J*. *Phys*. *Chem*. A, **1998**, *102*, 3470–3480.
[45] M. J. Romão, M. Archer, I. Moura, J. J. G. Moura, J. LeGall, E. Engh, M. Schneider, P. Hof and R. Huber, Crystal structure of the xanthine oxidase related aldehyde oxidoreductase from D. gigas, *Sci*. **1995**, *270*, 1170–1176.
[46] C. Kisker, H. Schindelin and D. C. Rees, Molybdenumcofactor–containing enzymes: structure and mechanism, *Annu*. *Rev*. *Biochem*. **1997**, *66*, 233–267.
[47] R. Huber, P. Hof, R. O. Duarte, J. J. G. Moura, I. Moura, M. Y. Liu, J. LeGall, R. Hille, M. Archer and M. J. Romão, A structure based catalytic mechanism for the xanthine oxidase family of molybdenum enzymes, *Proc*. *Natl*. *Acad*. *Sci*. **1996**, *93*, 8846–8851.
[48] M. J. Romão, J. Knäblein, R. Huber and J. J.G. Moura, Structure and Function of Molybdopterin Containing Enzymes, *Prog*. *Biophys*. *Molec*. *Biol*. **1997**, *68*, 121–144.
[49] K. N. Degtyarenko, A. C. T. North and J. B. C. Findlay, PROMISE: a database of bioinorganic motifs, *Nucleic Acids Res*. **1999**, *27*, 233–236.